Solution NMR Study of the Electronic Structure and Magnetic Properties of Cluster Ligation Mutants of the Four-Iron Ferredoxin from the Hyperthermophilic Archaeon *Pyrococcus furiosus*

Luigi Calzolai,[‡] Carol M. Gorst,[‡] Kara L. Bren,[†,‡] Zhi-Hao Zhou,[§]
Michael W. W. Adams,[§] and Gerd N. La Mar*,[‡]

Contribution from the Department of Chemistry, University of California,
Davis, California 95616, and Department of Biochemistry and Molecular Biology,
Center for Metalloenzyme Studies, University of Georgia, Athens, Georgia 30602

Received May 12, 1997. Revised Manuscript Received August 7, 1997[⊗]

Abstract: ^{1}H NMR is used to characterize the solution electronic structure and magnetic properties of the cubane iron−sulfur clusters for wild-type (WT) and the D14C and D14S cluster ligand mutants of the ferredoxin (Fd) from the hyperthermophilic archaeon *Pyrococcus furiosus* with the goal of identifying the oxidation states of the individual iron ligated by a particular protein ligand. Sequence-specific assignments of the contact-shifted and paramagnetically relaxed protons for all cluster ligands are obtained in the alternate cluster oxidation states, $[4Fe:4S]^+$, $[4Fe:4S]^{2+}$, each with Cys21 and Cys48 either as free sulfhydryls or in a disulfide bond. Detailed analysis of the oxidized cluster Fds shows that the ground state is $S = 0$ with similar population of excited $S = 1$ and 2 states for each of Asp14, Ser14, or Cys14 ligated to the cluster. The reduced cluster D14C Fd exhibits pairs of Cys (Cys11,Cys17) with strong Curie, and pairs of Cys (Cys14, Cys56) with strong anti-Curie temperature dependence diagnostic of ligands to the $S = {}^9/_2$, $2Fe^{2.5+}$, and $S = 4$, $2Fe^{2.0+}$ iron pairs, respectively. Moreover, it is observed that the ligand protons of Cys ligated to the mixed-valence pair are much more effectively relaxed than the Cys ligated to the diferrous pair, which is consistent with expectations for the relative spin magnetizations of the iron pair. Substitution of Cys14 by Ser14 leads to changes in contact shift magnitudes and slopes in Curie plots that demonstrate the presence of two electronic states that interchange the sequence positions of the $2Fe^{2.5+}$ and $2Fe^{2.0+}$. Similarly, replacement of Cys14 by Asp14 leads to changes in shift magnitude and Curie slope that indicate the population of two states for which the Asp14 is ligated to a $Fe^{2.5+}$ and Cys11 is ligated to a $Fe^{2.0+}$ in each state, while the other two ligands showed effective oxidation states midway between $Fe^{2.5+}$ and $Fe^{2.0+}$. Thus the relative stabilization of the mixed-valence pair for the iron ligated by residue 14 is Asp > Ser > Cys. The localization of the mixed-valence pair to the irons ligated to Cys11 and 17 in both D14C- and D14S-Fd is significantly stabilized for the disulfide relative to the free sulfhydryl form of Cys21 and Cys48, and likely reflects on a hydrogen bond between the backbones of Cys17 and Cys21. Ligation by cyanide in reduced WT Fd yields a contact shift pattern indicative of the same electronic state as for the Cys14 mutant, with cyanide ligated to one of the $2Fe^{2.0+}$. The conversion of a $Fe^{2.5+}$ ligated by Asp in WT Fd to a $Fe^{2.0+}$ upon cyanide displacement of the Asp is consistent with EPR and ENDOR studies (Telser, et al. *J. Am. Chem. Soc.* **1995**, *117*, 5133−5140; Telser et al., submitted for publication).

Introduction

The cubane or "bacterial-type" ferredoxins, Fds,[1] are small (∼60 residue) electron-transfer proteins that possess either 4Fe:4S or 3Fe:4S clusters that participate in electron-transfer reactions.[2] These clusters also occur as internal electron-transfer components in several larger redox enzymes such as nitrogenase[3] and hydrogenase.[4] They differ from the "plant-type" or 2Fe:2S Fd in that valence is shared by pairs of iron in cubane clusters $[2Fe^{2.5+}:2Fe^{2.5+}]^{2+}$ with $S = 0$, and $[2Fe^{2.5+}:2Fe^{2.0+}]^+$ with S

$= {}^1/_2$,[5] while the 2Fe Fd irons exhibit discrete valence, $[Fe^{3+}:Fe^{3+}]^{2+}$ with $S = 0$, and $[Fe^{3+}:Fe^{2+}]^+$ with $S = {}^1/_2$.[6,7] Shared valence is an intrinsic property of the cubane cluster[8,9] and manifests itself similarly in the high-potential iron proteins (Hipips),[10] but with more oxidized forms of the cluster, *i.e.*, $[2Fe^{2.5+}:2Fe^{2.5+}]^{2+}$ with $S = 0$ and $[2Fe^{2.5+}:2Fe^{3.0+}]^{3+}$ with $S = {}^1/_2$. The 4Fe:4S clusters that participate in catalysis in nonredox enzymes such as aconitase[11] and other hydratases[12] utilize solely the +2 oxidation state of the cluster. The $[4Fe:4S]^{2+}$

[†] Present address: Department of Chemistry, University of Rochester, Rochester, NY 14627.

[‡] University of California, Davis.

[§] University of Georgia.

[⊗] Abstract published in *Advance ACS Abstracts,* September 15, 1997.

(1) Abbreviations: *Pf, Pyrococcus furiosus*; Fd, ferredoxin; Hipip, high potential iron−sulfur protein; NOESY, 2D nuclear Overhauser spectroscopy; TOCSY, 2D total correlation spectroscopy; MCOSY, 2D magnitude correlation spectroscopy.

(2) Howard, J. B.; Rees, D. C. *Adv. Protein Chem.* **1991**, *42*, 199−280. Matsubara, H.; Saeki, K. *Adv. Inorg. Chem.* **1992**, *38*, 223−279. Cammack, R. *Adv. Inorg. Chem.* **1992**, *38*, 281−322. Johnson, M. K. In *Encyclopedia of Inorganic Chemistry*, King, R. B., Ed.; J. Wiley: New York, 1994; pp 1896−1915.

(3) Howard, J. B.; Rees, D. C. *Chem. Rev.* **1996**, *96*, 2965−298.

(4) Volbeda, A.; Charon, M.-H.; Piras, C.; Hatchikian, E. C.; Frey, M.; Fontecilla-Camps, J. C. *Nature* **1995**, *373*, 580−587.

(5) Moss, T. H.; Bearden, A. J.; Bartsch, R. G.; Cusanovich, M. A.; San Pietro, A. *Biochemistry* **1968**, *7*, 1591−1596. Cammack, R.; Dickson, D.; Johnson, C. In *Iron Sulfur Proteins*, Lovenberg, W., Ed.; Academic Press: New York, 1977; pp 283−330. Middleton, P.; Dickson, D. P. E.; Johnson, C. E.; Rush, J. D. *Eur. J. Biochem.* **1978**, *88*, 135−141.

(6) Gibson, J. F.; Hall, D. O.; Thornley, J. H. M.; Wheatley, F. R. *Proc. Natl. Acad. Sci. U.S.A.* **1966**, *56*, 987−992. Johnson, C. E. *J. Inorg. Biochem.* **1986**, *28*, 207−0215.

(7) Dunham, W. R.; Palmer, G.; Sands, R. H.; Bearden, R. J. *Biochem. Biophys. Acta* **1971**, *253*, 373−384.

(8) Holm, R. H.; Ibers, J. A. in *Iron Sulfur Proteins*; Lovenberg, W., Ed.; Academic Press: New York, 1977; Vol. III, pp 206−281.

(9) Bominaar, E. L.; Borshch, S. A.; Girerd, J.-J. *J. Am. Chem. Soc.* **1994**, *116*, 5362−5372.

and [2Fe:2S]$^{2+}$ clusters possess diamagnetic spin ground states, but have moderate antiferromagnetic coupling constants that lead to significant populations of $S = 1$, $S = 2$, etc., excited states at ambient temperature. The nature of protein interactions that determine the highly variable overall cluster reduction potential and discriminate among the reduction potentials of individual iron or pairs of iron within a cluster is the focus of significant theoretical and experimental investigation.[13]

While Mössbauer spectroscopy demonstrates the presence of mixed-valence pairs of iron in [4Fe:4S]$^{+}$, [3Fe:4S]^{0}, and [4Fe:4S]$^{3+}$ clusters,[5,10,14] the identification of the specific iron ligated to each Cys in the protein sequence that form the mixed-valence pair is uniquely addressable by NMR,[7,15−17] where the contact shift, δ_{con}, directly senses $\langle S_z \rangle$ for a given iron via:

$$\langle S_z \rangle \propto \frac{\delta_{con}}{A_i f(\theta)} \qquad (1)$$

where A_i is the hyperfine coupling constant for a $C_\beta H$ and $f(\theta)$ is an angular term related to the Fe−S−C_β−H dihedral angle.[18] Thus the pairwise valence delocalization and antiferromagnetic coupling are expected to lead to spin magnetization on pairs of Fe in these clusters (and hence the contact shifts of the ligands) which exhibit low-field Curie-like behavior (positive slope in a plot of contact shift vs reciprocal temperature) for the mixed-valence pair 2Fe$^{2.5+}$ in each of [4Fe:4S]$^{+}$ and [3Fe:4S]^{0}. On the other hand, the ligand(s) to the 2Fe$^{2.0+}$ and Fe$^{3.0+}$, respectively, are expected to exhibit anti-Curie (negative slope) behavior in a Curie plot.[16,18] Although the overwhelming majority of Fe-S clusters are ligated by Cys, there are now several documented cases of naturally occurring non-Cys ligation. Prominent examples are the hydratases such as aconitase,[11,19] (4Fe:4S with three Cys, one OH^{-}), the Rieske protein[20] (2Fe:2S; two Cys, two His), Ni-hydrogenase[4] (4Fe:4S; three Cys, one His) and the Fd from the hyperthermophile,[21−24] *Pyrococcus furiosus*, *Pf* (4Fe:4S with three

(10) Dickson, D. P. E.; Johnson, C. E.; Commack, R.; Evans, M. C. J.; Hall, D. O.; Rao, K. K. *Biochem. J.* **1974**, *139*, 105−108. Carter, C. W., Jr. *J. Biol. Chem.* **1977**, *252*, 7802−7811. Middleton, P.; Dickson, D. P. E.; Johnson, C. E.; Rush, J. D. *Eur. J. Biochem.* **1980**, *104*, 289−296. Mouesca, J.-M.; Rius, G.; Lamotte, B. *J. Am. Chem. Soc.* **1993**, *115*, 4714−4731.
(11) Beinert, H.; Kennedy, M. C.; Stout, C. D. *Chem. Rev.* **1996**, *96*, 2335−2373.
(12) Flint, D. H.; Allen, R. *Chem. Rev.* **1996**, *96*, 2315−2334.
(13) Mouesca, J.-M.; Chen, J. L.; Noodleman, L.; Bashford, D.; Case, D. A. *J. Am. Chem. Soc.* **1994**, *116*, 11898−11914. Stephens, P. J.; Jolie, D. R.; Warshel, A. *Chem. Rev.* **1996**, *96*, 2491−2513.
(14) Münck, E.; Papaefthymiou, V.; Sererus, K. K.; Girerd, J.-J. (1988) In *Metal Clusters in Proteins*, Que, L., Ed.; ACS Symposium Series; American Chemical Society: Washington, DC, 1988; pp 302−325.
(15) Dugad, L. B.; La Mar, G. N.; Banci, L.; Bertini, I. *Biochemistry* **1990**, *29*, 2263−2271.
(16) Bertini, I.; Ciurli, S.; Luchinat, C. *Struct. Bond.* **1995**, *83*, 1−54.
(17) Cheng, H.; Markley, J. L. *Annu. Rev. Biophys. Biomol. Struct.* **1995**, *24*, 209−237.
(18) Phillips, W. D.; Poe, M. In *Iron Sulfur Proteins*; Lovenberg, W., Ed.; Adacemic Press: New York; Vols. I and II (1973); Vol. III, pp 255−285 (1977). Bertini, I.; Capozzi, F.; Luchinat, C.; Piccioli, M.; Vila, A. J. *J. Am. Chem. Soc.* **1994**, *116*, 651−660. Noodleman, L.; Chen, T.-L.; Case, D. A.; Giori, C.; Rius, G.; Mouesca, J.-M.; Lamotte, B. In *Nuclear Magnetic Resonance of Paramagnetic Macromolecules*; La Mar, G. N., Ed.; Kluwer Press: Dordrecht, NL, 1995; pp 339−367.
(19) Werst, M. M.; Kennedy, M. C.; Beinert, H.; Hoffman, B. M. *Biochemistry* **1990**, *29*, 10526−10532.
(20) Fee, J. A.; Findling, K. L.; Yoshida, T.; Hille, R.; Tarr, G. E.; Hearshen, D. O.; Dunham, W. R.; Day, E. P.; Kent, T. A.; Münck, E. *J. Biol. Chem.* **1984**, *259*, 124−133.
(21) Aono, S; Bryant, F. O.; Adams, M. W. W. *J. Bacteriol.* **1989**, *171*, 3433−3439.
(22) Conover, R. C.; Park, J.-B.; Adams, M. W. W.; Johnson, M. K. *J. Am. Chem. Soc.* **1991**, *113*, 2799−2800.
(23) Adams, M. W. W. *Adv. Inorg. Chem.* **1992**, *38*, 341−396.
(24) Calzolai, L.; Gorst, C. M.; Zhao, Z.-H.; Teng, Q.; Adams, M. W. W.; La Mar, G. N. *Biochemistry* **1995**, *34*, 11373−11384.

Cys, one Asp). The P cluster in nitrogenase has been shown to possess one ligated Ser in the oxidized form of the cluster.[25] In several cases, the absence of a Cys in the cluster ligating consensus sequence of a Fd suggests non-Cys ligation,[26] but the nature of the ligand is to be determined. Non-Cys cluster ligands are conventionally identified in X-ray structure or by EPR/ENDOR,[19,27] but can also be identified by solution ^1H NMR.[24]

Attempts to introduce non-Cys ligands into ferredoxins and Hipips by site-directed mutagenesis,[28,29] and their subsequent characterization by ^1H NMR,[30−32] have met with limited success. For example, Cys to Ser substitution at the four positions in *Chromatium vinosum* Hipip allowed the isolation of only one protein, that with C77S substitution.[32] On the other hand, Cys to Ser substitution of the four Cys cluster ligands in the *Anabaena* 2Fe Fd allowed the ^1H NMR characterization of all four mutants of the oxidized protein and of two mutants in the reduced form.[30,31] Since the protein−cluster bonds contribute significantly to the folding free energy of most Fd,[30−32] the reduced stability of a non-Cys−iron bond may preclude the systematic perturbation of the individual four ligands. The cubane Fds from hyperthermophiles[23] are ideal candidates for such mutation/NMR studies. First, WT *Pf* Fd already possesses[24] a ligated Asp14, and recent mutagenesis experiments have provided stable Fds with the Asp14Cys or Asp14Ser mutations.[33] The ability to probe three cluster ligand types, Asp, Ser, and Cys, currently unique to *Pf* Fd, is further extended by the ability of a cyanide ion to ligate to the cluster[22,27] in the reduced 4Fe *Pf* Fd.

A complicating feature of *Pf* Fd is that both the 4Fe:4S cluster and a pair of remote Cys (Cys21 and Cys48) are redox active at approximately the same potential. When operating at ambient temperatures, some ∼70−80 °C below the functioning temperature of the organism *Pf* (optimal growth temperature 100 °C), the 2SH ↔ −S−S− reaction is extremely slow, affording four distinct redox states of *Pf* Fd that can be characterized.[34] A schematic representation of the *Pf* 4Fe Fd is given in Figure 1, where the A and B states (labeled as subscripts) correspond to the disulfide and free sulfhydryl forms of Cys21,48, respectively. Together with the oxidized and reduced states of the cluster, Fd^{ox}, [4Fe:4S]$^{2+}$, and Fd^{red}, [4Fe:4S]$^{1+}$, respectively, *Pf* Fd exists in four distinct states identified as Fd$_A^{red}$, Fd$_B^{red}$, Fd$_A^{ox}$, and Fd$_B^{ox}$. We present herein the results of a ^1H NMR study designed to answer the following questions: What is the effect of non-Cys ligation on the electronic/magnetic properties of the cluster? How does the nature of the position-14 ligand influence the oxidation state of its coordinated iron? Can the ^1H NMR hyperfine shift pattern alone provide evidence for non-Cys

(25) Peters, J. W.; Stowell, M. H. B.; Soltis, S. M.; Finnegan, M. G.; Johnson, M. K.; Rees, D. C. *Biochemistry* **1997**, *36*, 1181−1187.
(26) George, S. J.; Armstrong, F. A.; Hatchikian, E. C.; Thomson, A. J. *Biochem. J.* **1989**, *264*, 275−284. Meyers, J.; Fujinga, J.; Gaillard, J.; Lutz, M. *Biochemistry* **1994**, *33*, 13642−13650. Yu, L.; Bryant, D. A.; Golbeck, J. H. *Biochemistry* **1995**, *34*, 7861−7868. Yu, L.; Vassiliev, I. R.; Jung, Y.-S.; Bryant, D. A.; Golbeck, J. H. *J. Biol. Chem.* **1995**, *270*, 28118−28125.
(27) Telser, J.; Smith, E. T.; Adams, M. W. W.; Conover, R. C.; Johnson, M. K.; Hoffman, B. M. *J. Am. Chem. Soc.* **1995**, *17*, 5133−5140.
(28) Moulis, J.-M.; Davasse, V.; Golinelli, M.-P.; Meyer, J.; Quinkal, I. *J. Biol. Inorg. Chem.* **1996**, *1*, 2−14.
(29) Feinberg, B. A.; Lo, X.; Iwamoto, T.; Tomich, J. M. *Protein Eng.* **1997**, *10*, 69−75.
(30) Cheng, H.; Xia, B.; Reed, G. H.; Markley, J. L. *Biochemistry* **1994**, *33*, 3155−3164.
(31) Holden, H. M.; Jacobson, B. H.; Hurley, J. K.; Tollin, G.; Oh, B.-H.; Skjeldal, L.; Chae, Y. K.; Cheng, H.; Xia, B.; Markley, J. L. *J. Bioinorg. Biomembr.* **1994**, *26*, 67−88.
(32) Babini, E.; Bertini, I.; Borsari, M.; Capozzi, F.; Dikiy, A.; Eltis, L. D.; Luchinat, C. *J. Am. Chem. Soc.* **1996**, *118*, 75−80.
(33) Zhou, Z.-H.; Adams, M. W. W. *Biochemistry* **1997**, submitted.
(34) Gorst, C. M.; Zhou, Z.-H.; Ma, K.; Teng, Q.; Howard, J. B.; Adams, M. W. W.; La Mar, G. N. *Biochemistry* **1995**, *34*, 8788−8795.
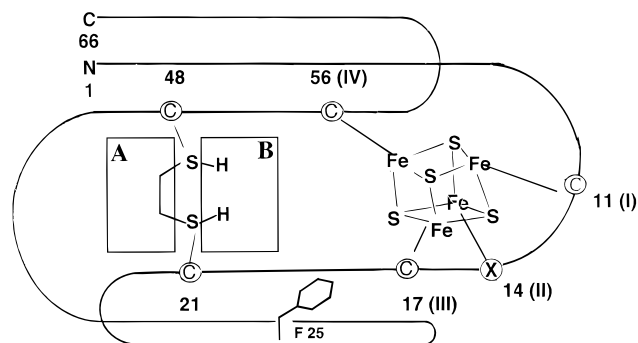
Figure 1. Schematic representation of the molecular structure of a cubane single-cluster Fd (adapted from ref 2). The cluster ligands are labeled by both the conserved ligation sequence I−IV and the sequence position in *Pf* Fd, 11, 14, 17 and 56, with position 14(II) occupied by Asp in WT *Pf* Fd. The alternate oxidation states of the two Cys21 (V), Cys48 (VI) remote from the cluster, two free sulfhydryl and a disulfide bond, are designated by the B and A form, respectively. These, together with the two cluster oxidation states, generate the four redox states Fd_A^{ox}, Fd_B^{ox}, Fd_A^{red}, and Fd_B^{red}. The proximity of Phe25 to Cys17 (**III**) used in the assignments, is also shown.

ligation? What influence do the remote sulfhydryls have on the cluster magnetic properties?

Experimental Section

Proteins. *Pyrococcus furiosus* 4Fe Fd was purified as previously reported.[21] The recombinant mutant Fds, Asp14Cys, and Asp14Ser were obtained from *E. coli* as described elsewhere.[33] All *Pf* Fds were purified under anaerobic and reducing conditions, yielding the cluster reduced and free thiol Cys21,-48 form of the protein referred to as Fd_B^{red}. All protein samples for NMR were handled in a Vacuum Atmospheres inert atmosphere glovebox. Starting with the as-isolated Fd_B^{red} ([4Fe:4S]$^+$, SH, SH), controlled conversion to the sequential redox states Fd_B^{ox} ([4Fe:4S]$^{2+}$, SH, SH), Fd_A^{ox} ([4S:4S]$^{2+}$, S−S), Fd_A^{red} ([4Fe:4S]$^+$, S−S), and finally to Fd_B^{red} again to close the redox cycle, were carried out using O_2 as oxidant and dithionite as reductant, as described in detail previously.[34] Solutions of the desired Fd form were prepared in ^1H_2O or ^2H_2O with either 50 or 300 mM phosphate (to reduce or accelerate, respectively, the electron self-exchange rates[35] between [4Fe:4S]$^{2+}$ and [4Fe:4S]$^+$ at pH 7.2. Samples of Fd_B^{red} and Fd_A^{ox} were prepared at pH values 6.0, 7.2, and 8.0. The ligation of cyanide to Fd_B^{red} and Fd_A^{red} was investigated by addition of KCN (100 and 500 mM) to 3 mM Fd^{red} in 50 mM tris, at pH 8.0.[22]

NMR Spectroscopy. All ^1H NMR spectra were recorded at 500 MHz on a GE Omega 500 spectrometer. Chemical shift values were referenced to 2,2-dimethyl-2-pentane-5-sulfonate, DSS, through the residual solvent signal. Spectra were collected over a range of temperature and pH (6.0−8.6) by the normal one-pulse sequence with ^1H_2O presaturation using a long recycle time (3 s), or with the super-WEFT pulse sequence[36] utilizing a shorter recycle time (∼180 ms). Nonselective T_1s were obtained from the initial slope of the recovery of magnetization after an inversion−recovery pulse sequence; recycle times were set at ∼5 times the T_1 for the peaks of interest. Magnetization-transfer experiments to detect either steady-state NOE or chemical exchange were performed using a super-WEFT pulse sequence.[24] The selected resonance was irradiated for ∼90% of the relaxation delay time. Geminal and vicinal protons were differentiated by the different cross relaxation rate σ_{ij}; the estimated rotational correlation time τ_c of 3 ns predicts $\sigma_{ij} \cong 5$

s^{-1} for geminal and $\sigma_{ij} \cong 1$ s^{-1} for vicinal protons.[24] Phase-sensitive TOCSY[37] and NOESY[38] spectra were recorded at 30 and 40 °C using spin lock times of 15 and 60 ms for TOCSY and mixing times of 50 or 250 ms for NOESY over a 7017 Hz sweepwidth. The 60 ms TOCSY and 250 ms NOESY spectra consisted of 96 scans collected at a repetition rate of 0.5 s^{-1}, the 15 ms TOCSY consisted of 256 scans collected at a repetition rate of 1.3 s^{-1} and the 50 ms NOESY consisted of 160 scans collected at a repetition rate of 0.7 s^{-1}; all with 2048 complex t_2 points over 512 t_1 blocks. The water signal was suppressed by low-power selective irradiation during the pre-delay period for all experiments. MCOSY[39] spectra are recorded over 27 kHz with a repetition rate of 3 s^{-1} using 1024 scans per block. NMR data were processed on a Silicon Graphics Indigo2 workstation using the Biosym/Molecular Simulations Felix 95.0 program. Sine-bell-squared functions, 30° shifted, were applied in both dimensions for NOESY and TOCSY data. Data sets were zero-filled to 2048 × 2048 real data points prior to Fourier transformation.

Results

The ^1H NMR spectra in the "diamagnetic" 0−10 ppm window for the two mutants Fd^{ox} are essentially the same as that of WT Fd as reported previously.[35] Partial analysis of 2D NMR data in a manner described in detail[40] for 3Fe *Pf* Fd_A^{ox} reveal very similar cross peak patterns (not shown) that reflect conservation of the folding in the two mutants (*i.e.,* contacts between Val24 and Phe25 and between Trp2 and Tyr46 are completely conserved). The folding pattern reflected in these tertiary contacts has been shown[34] to be similarly conserved between WT Fd_A^{ox} and WT Fd_B^{ox}. The chemical shifts for several key residues are listed in Supporting Information.

Identification of Multiple Oxidation States. The four oxidation states of WT *Pf* Fd, designated Fd_A^{ox}, Fd_B^{ox}, Fd_A^{red}, and Fd_B^{red}, exhibit resonances labeled A_i^o, B_i^o, A_i^r, and B_i^r, respectively, with the subscript *i* labeled so that it represents the same proton in the same ligand for both the mutants and WT Fd.[24,34] The two mutants, D14C and D14S can be prepared under controlled conditions in either A or B forms for both cluster oxidation states, as described in detail previously for WT *Pf* Fd.[34] The cyanide-ligated Fd^{red} can be converted between the A and B forms in an analogous fashion. The low-field hyperfine-shifted portions of the ^1H NMR spectra for the oxidized Fds are shown in Figure 2. The spectra in parts A−C of Figure 2 show the gradual conversion of D14C Fd_B^{ox} to D14C-Fd_A^{ox} in the presence of O_2. As was noted in WT *Pf* Fd,[24,34] only one ligand proton yields clearly resolved signals for the A and B forms, that labeled A_1^o, B_1^o in Figure 2 where superscript "o" designates oxidized; the intensities of the remaining resonances, as in the case of WT Fd, show that the A_i^o, and B_i^o peaks for any i $\neq 1$ are generally degenerate. The ^1H NMR spectra in Figure 2D,E depict the similar conversion of D14S-Fd_B^{ox} to D14S-Fd_A^{ox}; in this case, the A_5^o, and B_5^o, and A_9^o and B_9^o peaks are also partially resolved. A spectrum of WT 30% Fd_A^{ox} and 70% Fd_B^{ox} is shown as a reference in Figure 2F. The solid lines connect the signals for Fd_A^{ox} that will be shown to arise from the same proton on the identical Cys, while a dashed line connects the resonances that will be demonstrated to arise from the variable position-14 cluster ligand. The chemical shifts and nonselective T_1 values of the ligand resonances for WT and mutant Fd_A^{ox} and Fd_B^{ox}

(35) Calzolai, L.; Zhou, Z.-H.; Adams, M. W. W.; La Mar, G. N. *J. Am. Chem. Soc.* **1996**, *118*, 2513−2514.

(36) Inubushi, T.; Becker, E. D. *J. Magn. Reson.* **1983**, *51*, 128−133.

(37) Bax, A.; Davis, D. G. *J. Magn. Reson.* **1985**, *65*, 355−360.

(38) Jeener, J.; Meier, B. H.; Bachmann, P.; Ernst, R. R. *J. Chem. Phys.* **1979**, *71*, 4546−4553.

(39) Bax, A. *Two Dimensional NMR in Liquids*; Reidel Publishing Co.: Dordrecht, The Netherlands, 1982.

(40) Teng, Q.; Zhou, Z.-H.; Smith, E. T.; Busse, S. C.; Howard, J. B.; Adams, M. W. W.; La Mar, G. N. *Biochemistry* **1994**, *33*, 6316−6326.
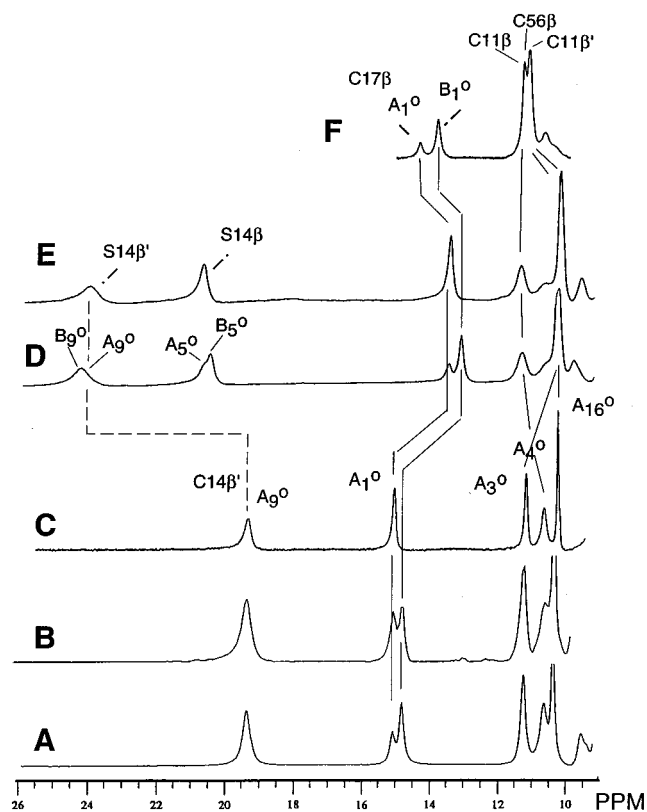
Figure 2. Resolved low-field portions of the 500 MHz ^{1}H NMR spectra (repetition rate 4 s^{-1}) of 5−8 mM *Pf* Fd^{ox} in 90% ^{1}H$_2$O:10% ^{2}H$_2$O, 50 mM phosphate, pH 7.2 at 30 °C for (A−C) D14C-Fd^{ox} showing the slow conversion of D14C-Fd$_B^{ox}$ (peak labeled B$_i^o$) to D14C-Fd$_A^{ox}$ (peak labeled A$_i^o$) in the presence of O$_2$, (D and E) D14S-Fd^{ox} showing the conversion of D14S-Fd$_B^{ox}$ to D14S-Fd$_A^{ox}$ in the presence of O$_2$; and (F) WT-Fd with 30% Fd$_A^{ox}$ and 70% Fd$_B^{ox}$ present. The peaks for Fd$_A^{ox}$ and Fd$_B^{ox}$ are labeled A$_i^o$ and B$_i^o$, respectively if the two resonances are resolved or partially resolved; in the majority of cases where A$_i^o$ and B$_i^o$ for the same i are degenerate, only A$_i^o$ is labeled.

are listed in Table 1. The temperature behavior for all protons in both mutant Fd^{ox} is anti-Curie (negative slope in Curie plot in both mutants) and is essentially the same as found previously[34] for WT *Pf* Fd^{ox} (not shown; see Supporting Information) and other [4Fe:4S]$^{2+}$ proteins.[16,17]

The ^{1}H NMR spectra for the reduced cluster species in primarily the B form of WT Fd, D14C-Fd, and D14S-Fd are illustrated in parts A, B, and C of Figure 3, respectively, with peaks labeled B$_i^r$ (labeled in Figure 3A) for each protein. As found[24,34] for the WT Fd^{red}, the pattern of hyperfine shifts can differ sufficiently between the A and B forms to allow resolution of all signals at an appropriate temperature. The same index *i* is used to label a unique proton in a given ligand (to be demonstrated below) in all four oxidation states of each Fd. To avoid crowding, only B$_i^r$ peaks are labeled in Figure 3A and the positions of all A$_i^r$ peaks are indicated by asterisks. The detailed labeling of the A$_i^r$ peaks in the same spectra is given in Supporting Information. The chemical shifts and nonselective T_1s for ligand resonances in the mutant Fd^{red} complex are listed in Table 2 where they can be compared to similar data[24] on WT Fd^{red}. The temperature dependences for the cluster ligand proton chemical shifts are shown in the form of a Curie plot (observed chemical shift versus reciprocal absolute temperature) for D14C-Fd$_A^{red}$ (closed markers) and D14S-Fd$_A^{red}$ (open markers) in Figure 4A, and for D14C-Fd$_B^{red}$ (closed markers) and D14S-Fd$_B^{red}$ (open markers) in Figure 4B. The variable-temperature data for WT Fd$_A^{red}$ and Fd$_B^{red}$, some of which was reported previously,[24,34] are given in Supporting Information.

The ^{1}H NMR spectrum of a sample ∼75% WT Fd$_B^{red}$-CN (peaks labeled B$_i^{CN}$) and ∼25% unreacted WT Fd$_B^{red}$ (positions marked by filled squares) is shown in Figure 3D and reveals five resolved low-field peaks for Fd$_B^{red}$-CN. Two assignable signals (see below) are labeled B$_1^{CN}$ and B$_6^{CN}$ (and connected by solid lines to the same proton peaks in the other spectra). The three remaining signals are labeled B$_x^{CN}$, B$_y^{CN}$, and B$_z^{CN}$. The spectrum for WT Fd$_A^{red}$-CN is provided in Supporting Information. Both the chemical shifts and T_1s for the ligated Cys in Fd^{red}-CN are given in Table 3. Curie plots for WT Fd$_B^{red}$-CN and WT Fd$_A^{red}$-CN, are given in Supporting Information.

Assignment of Cluster Ligand Resonances. The cluster ligand assignments are based on the use of the 1D and 2D NMR methods optimized for relaxed protons[41] using the assignment protocol presented in detail for WT *Pf* Fd.[24,42] Single cubane cluster Fd have in common a conserved cluster geometry that allows the detection of narrow ^{1}H NMR signals for the N$_p$H, but not C$_\alpha$H, of Cys I and Cys IV, and for the C$_\alpha$H, but not N$_p$H, of Cys III (and ligand II).[24,42] Dipolar contacts to adjacent residues (Thr10 and Ser59) differentiate Cys I and Cys IV, while Cys III is uniquely identified by its proximity to a completely conserved Phe25 (see Figure 1). Assignments for the mutant Fds were initially carried out independently on relatively pure Fd$_A^{ox}$ and Fd$_B^{red}$, and the assignments subsequently extended to Fd$_A^{red}$ and Fd$_B^{ox}$, respectively, by magnetization transfer, as reported earlier for WT *Pf* Fd.[24]

D14C-Fd. A COSY spectrum for D14C-Fd$_A^{ox}$ exhibits cross peaks for each of the five resolved hyperfine shifted resonances that locate the following three three-spin systems: (A$_1^o$,A$_6^o$,A$_7^o$), (A$_9^o$,A$_5^o$,A$_{16}^o$), and (A$_3^o$,A$_{11}^o$,A$_{30}^o$) and one two-spin system (A$_2^o$,A$_4^o$) (not shown; see Supporting Information). The sequence-specific assignments, as well as the differentiation of C$_\alpha$H and C$_\beta$H signals of D14C-Fd$_A^{ox}$, are more conveniently carried out by steady-state NOEs.[24] Representative NOE data for D14C-Fd$_A^{ox}$ are illustrated in Figure 5. Saturation of A$_1^o$ yields a weak NOE to the strongly relaxed A$_7^o$ (not shown) and a stronger NOE to a weakly relaxed signal A$_6^o$ (Figure 5B), as well as to the assigned Phe25 ring proton and Leu20 N$_p$H which identifies A$_1^o$, A$_6^o$, and A$_7^o$ as the Cys17 C$_\beta$H, C$_\alpha$H, and C$_\beta$H′ (C$_\beta$H and C$_\beta$H′ are the Cys β-protons furthest from, and closest to, the ligated cluster iron, respectively). The saturation of peak A$_3^o$ (Figure 5C) yields an NOE to a strongly relaxed proton A$_{11}^o$, as well as two labile protons labeled a$_{17}^o$ and a$_{33}^o$. Peak a$_{33}^o$ has been identified as the Ser59 NH, which uniquely identifies A$_3^o$, A$_{11}^o$, and a$_{17}^o$ as the C$_\beta$H, C$_\beta$H′, and N$_p$H of Cys56. Saturation of A$_4^o$ yields NOEs to a strongly relaxed signal A$_2^o$ and two labile protons, one labeled a$_{15}^o$ and the other Thr10 N$_p$H (Figure 5D). These results clearly identify C$_\beta$′H, C$_\beta$H, and N$_p$H of Cys11. Finally, saturating the low-field A$_9^o$ results in NOEs to both a weakly relaxed peak A$_{16}^o$ and a more strongly relaxed signal A$_5^o$ which must arise from the C$_\beta$H′, C$_\alpha$H and C$_\beta$H of the remaining Cys14 (Figure 5E). The chemical shift and T_1 values are listed in Table 1.

The relevant steady-state NOE results for D14C-Fd$_B^{red}$ are illustrated in Figure 6. Saturation of B$_1^r$ results in NOEs to a broad peak B$_7^r$ and a narrow peak B$_6^r$, as well as to the Phe25 ring (Figure 6B), identifying Cys17 C$_\beta$H, C$_\beta$H′, and C$_\alpha$H, respectively. Saturation of B$_2^r$ (in the negative direction in Figure 6B) yields a significant NOE to a strongly relaxed proton peak B$_4^r$ identifying a geminal CH$_2$ for cluster ligand Cys11 or Cys56. Irradiation of B$_3^r$ (Figure 6D) yields a weak NOE to a strongly relaxed signal B$_{11}^r$ and to a slowly exchanging labile proton peak b$_{17}^r$, and identifies the C$_\beta$H, C$_\beta$H′, and N$_p$H of

(41) La Mar, G. N.; de Ropp, J. S. *Biol. Magn. Reson.* **1993**, *18*, 1−78.
(42) Gorst, C. M.; Yeh, T.; Teng, Q.; Calzolai, L.; Zhou, Z.-H.; Adams, M. W. W.; La Mar, G. N. *Biochemistry* **1995**, *34*, 600−610.

Table 1. ^{1}H NMR Spectral Propreties of the Cluster Ligands in Wild-Type and Position-14 Mutants of Oxidized *Pyrococcus furiosus* 4Fe Ferredoxin

ligand	assignment	peak label	WT[a]		D14C		D14S	
			$Fd_A^{ox\,b}$	$Fd_B^{ox\,b}$	Fd_A^{ox}	Fd_B^{ox}	Fd_A^{ox}	Fd_B^{ox}
Cys11 (**I**)	$C_\beta H$	A_2^o	11.3[c] (9)[e]	11.3 (10)	9.1 (17)[d]	9.1	10.0 (9)	10.0
	$C_\beta H'$	A_4^o	11.1 (3)[e]	11.1	10.9 (4)[e]	10.8	11.1 (3)	11.3
	$N_P H$	a_{15}^o	7.5	7.35/7.42	7.7		7.7	
ligand 14 (**II**)	$C_\beta H$	A_5^o	4.9	4.9	9.1 (13)[e]		20.1 (3)	20.7
	$C_\beta H'$	A_9^o	5.37 (15)	5.37	19.5 (6)	19.5	23.3 (2)	23.2
	$C_\alpha H$	A_{16}^o			10.5 (28)		8.2	
Cys17 (**III**)	$C_\beta H$	A_1^o	14.3 (6)	13.8	15.3 (9)	15.0	12.7 (6)	13.6
	$C_\beta H'$	A_7^o	5.9 (2)[e]	6.0	4.8			
	$C_\alpha H$	A_6^o	8.6 (33)	8.75	7.5 (36)		8.37	
Cys56 (**IV**)	$C_\beta H$	A_3^o	11.1 (9)[e]	11.1	11.5 (10)	11.5	10.2 (9)	10.2
	$C_\beta H'$	A_{11}^o	8.1 (4)	8.2	6.9 (2)			
	$C_\alpha H$	A_{30}^o			5.2			
	$N_P H$	a_{17}^o	7.5	7.42/7.35	7.4		7.21	

[a] Data taken from ref 24. [b] Subscripts A and B refer to disulfide bond and free sulfhydryl, respectively, for Cys21,48. [c] Chemical shifts, in ppm from DSS, in ^{1}H$_2$O at 30 °C. [d] Nonselective T_1, in ms, are given in parentheses for resolved peaks; uncertainties ±15% unless indicated otherwise. [e] Nonselective T_1, in ms, are given in parentheses for partially resolved peaks with uncertainties ±30%.
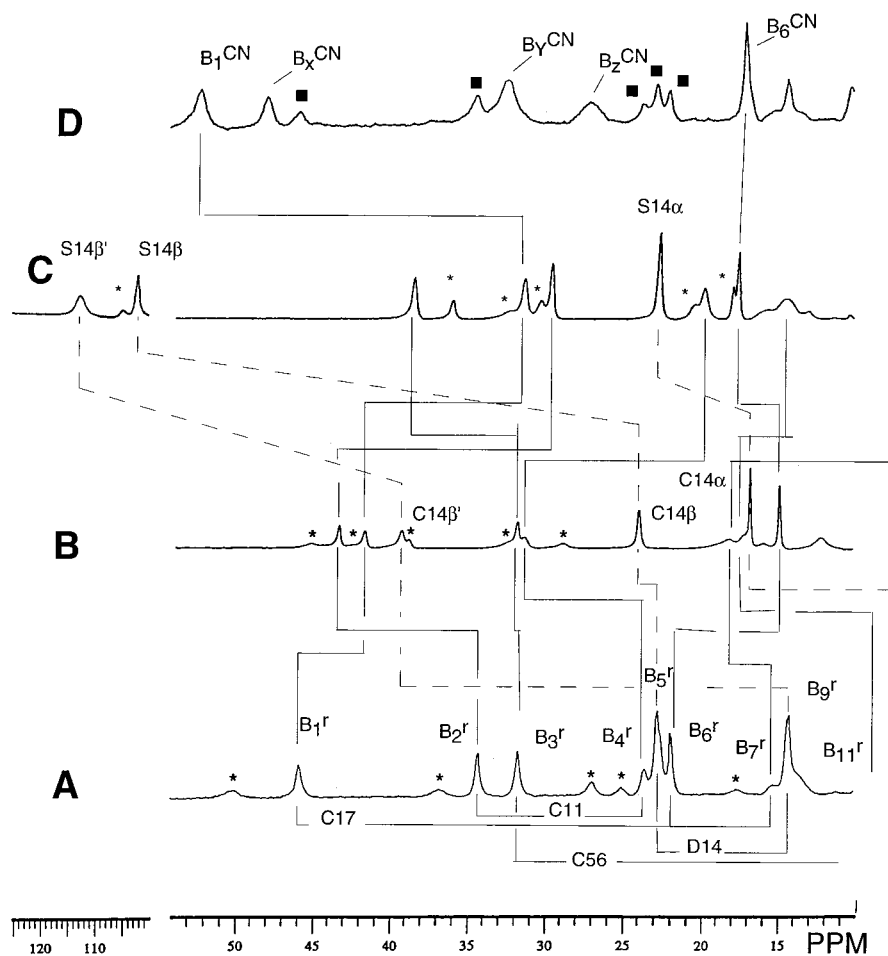

Figure 3. Resolved low-field portions of the 500 MHz ^{1}H NMR spectra (repetition rate 4 s^{-1}) in ^{2}H$_2$O, 50 mM phosphate at 30 °C of 3−5 mM of reduced cluster 4Fe *Pf* Fd predominantly in the B form (free sulfhydryl Cys21,48) for (A) WT Fd_B^{red}, (the label designation for contact shifted peaks, B_i^r, is shown above the spectrum and the sequence-specific assignment below the spectrum of WT *Pf* Fd_B^{red}), (B) D14C-Fd_B^{red}, (C) D14S-Fd_B^{red}, and (D) WT Fd_B^{red}-CN (positions of unreacted WT Fd_B^{red} peaks are indicated by filled squares). Peaks are labeled B_i^r for WT, D14C, and D14S-Fd, and B_i^{CN} for the cyanide-ligated WT Fd. Positions of the minor Fd_A^{red} form in each case are indicated by asterisks. Similarly labeled and assigned peaks for Cys11, 17, and 56 in B D are connected by solid lines. The variable-ligand 14 resonances are connected by dashed lines.

cluster ligand Cys56 or Cys11. Lastly, irradiation of B_9^r leads to a significant NOE to both a strongly relaxed peak B_5^r and a weakly relaxed peak B_{16}^r, which must arise from the $C_\beta H'$, $C_\beta H$, and $C_\alpha H$ of the remaining Cys14 (Figure 6C). The differentiation of the Cys11 vs Cys56 resonances in Fd_B^{red} was accomplished by observing saturation transfer[43] to the respective

resonances in Fd_B^{ox} with essentially the same shift as unambiguously determined above for Fd_A^{ox} (not shown; see Supporting Information). Similar saturation transfer between Fd_A^{red} and Fd_A^{ox} provides the unique assignment of Fd_A^{red} (not shown). The chemical shifts and relaxation properties for the reduced cluster ligands are listed in Table 2.

D14S-Fd. The severe sensitivity of D14S-Fd_B^{ox} to conversion to the 3Fe cluster[33] upon exposure to even small amounts

(43) Sandström, J. *Dynamic NMR Spectroscopy*; Academic Press: New York, 1982.

Table 2. ^{1}H NMR Spectral Parameters of the Cluster Ligands to Wild-Type and Position-14 Mutants of Reduced Cluster *Pyrococcus furiosus* 4Fe Ferredoxin

			WT[a]		D14C		D14S	
ligand	assignment	peak label	$Fd_B^{red\ b}$	$Fd_A^{red\ b}$	Fd_B^{red}	Fd_A^{red}	Fd_B^{red}	Fd_A^{red}
Cys11 (**I**)	$C_\beta H$	B_2^r	34.7[c] (19)[d]	37.4 (14)	43.5 (6)	45.3 (6)	30.0 (14)	30.7 (16)
	$C_\beta H'$	B_4^r	23.8 (9)	25.3 (6)	31.4 (3)	32.4 (3)	20.0 (6)	20.7 (5)
	$C_\alpha H$	B_{25}^r	−2.0 (3)					
	$N_P H$	b_{15}^r	7.61 (60)					
ligand 14 (**II**)	$C_\beta H$	B_5^r	22.7 (21)	22.8 (14)	24.0 (18)	24.0	105	~102
	$C_\beta H'$	B_9^r	14.3 (15)	14.4 (7)	39.4 (7)	39.0 (6)	113	~113
	$C_\alpha H$	B_{16}^r	7.46	7.38	16.8 (32)	16.8	22.9 (16)	22.9
Cys17 (**III**)	$C_\beta H$	B_1^r	45.8 (13)	50.2 (10)	41.8 (6)	42.7 (6)	31.8 (10)	32.7
	$C_\beta H'$	B_7^r	15.2 (3)	17.5 (3)	18.2 (3)		8	
	$C_\alpha H$	B_6^r	21.8 (29)	22.4 (21)	14.8 (24)		17.7 (22)	18.0 (22)
Cys56 (**IV**)	$C_\beta H$	B_3^r	31.6 (17)	27.0 (14)	31.9 (12)	28.9 (13)	39.1 (7)	36.5 (8)
	$C_\beta H'$	B_{11}^r	9.35 (<5)	7.5	17.2 (7)		14.2 (~3)[e]	
	$N_P H$	b_{17}^r	7.35 (60)					

[a] Data taken from ref 24. [b] Subscripts A and B refer to disulfide bond and free sulfhydryl, respectively, for Cys21,48. [c] Chemical shifts, in ppm from DSS, in [1]H₂O at 30 °C. [d] Nonselective T_1, in ms, for resolved peaks are given in parentheses, with uncertainties ±15% unless indicated otherwise. [e] Nonselective T_1, in ms, are given in parentheses for partially resolved peaks with uncertainties ±30%.
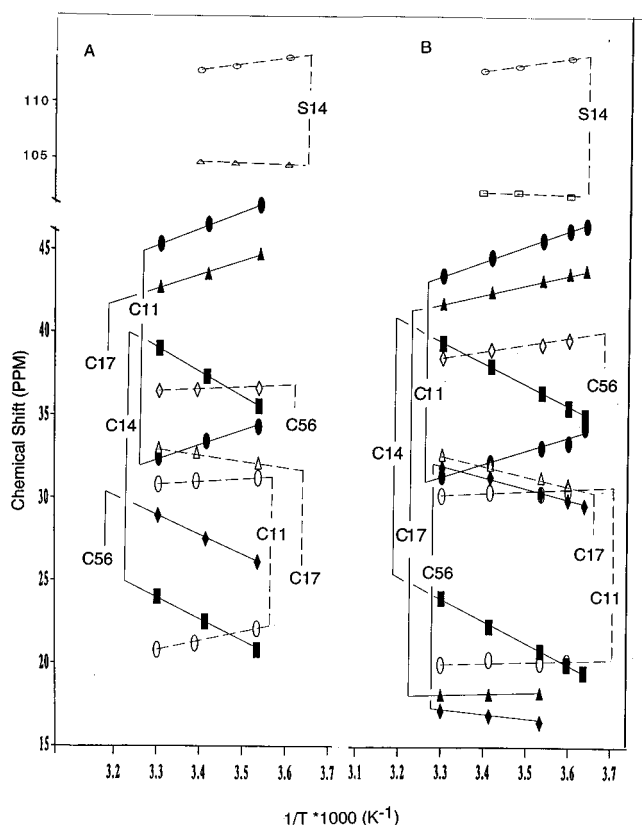

Figure 4. Curie plots (observed chemical shift vs reciprocal absolute temperature) for the low-field contact-shifted ligand protons for (A) D14C-Fd_A^{red} (closed markers) and D14S-Fd_A^{red} (open markers), and (B) D14C-Fd_B^{red} (closed markers) and D14S-Fd_B^{red} (open markers), all in ²H₂O, 50 mM in phosphate, pH 7.2. The proton peaks for Cys11, ligand 14, Cys17, and Cys56 are shown by circles, squares, triangles, and diamonds, respectively.

Table 3. ^{1}H NMR Spectral Properties of the Protein Ligands to the Reduced Cluster in Cyanide-Ligated Pyrococcus furiosus 4Fe Ferredoxin

		Fd_B^{red}-CN[a]		Fd_A^{red}-CN[a]	
ligand	assignment	peak label	shift[b] $(T_1)^c$	peak label	shift (T_1)
Cys17 (**III**)	$C_\beta H$	B_1CN	51.9[b] (<1)[d]	A_1CN	52.6 (<1)
	$C_\alpha H$	B_6CN	16.9 (14)[c]	A_6CN	16.5 (12)[c]
Cys11 (**I**)[e]	$C_\beta H'$	B_xCN	47.7 (<1)	A_xCN	51.1 (~1)[d]
	$C_\beta H$	B_yCN	32.3 (~1)[d]	A_yCN	34.5 (~1)[d]
Cys56 (**IV**)[e]	$C_\beta H$	B_zCN	26.7 (<1)	A_zCN	26.7 (<1)

[a] Subscripts A and B refer to disulfide bond and free sulfhydryl, respectively, for Cys21,48. [b] Chemical shifts, in ppm from DSS, in [1]H₂O at 30 °C. [c] Nonselective T_1, in ms, for resolved peaks are given in parentheses, uncertainty ±15%. [d] Estimates of nonselective T_1, in ms; uncertainty ±30%. [e] Tentative assignments based on comparison to WT Fd_B^{red}.

the ligated Cys in D14S-Fd_B^{ox} (not shown; see Supporting Information). The assignment of the key Ser signals in D14S-Fd_A^{red} is shown in parts E and D of Figure 7. Magnetization transfer[38] to A_9^o and A_5^o upon saturating A_9^r (Figure 7E) and A_5^r (Figure 7F), respectively, in a sample containing ~80% D14C-Fd^{ox} and ~20% D14S-Fd^{red}, with a $Fd_A:Fd_B$ ratio 70:30, identifies the signals with the unprecedented low-field hyperfine shifts as the $C_\beta H'$ $C_\beta H$ of Ser14. The nearly identical shifts for the A_5^o and B_5^o peaks, and the A_9^o and B_9^o peaks is apparent in parts D and E of Figure 2. Magnetization transfer from the remaining unassigned strongly hyperfine shifted peak B_{16}^r in D14S-Fd_B^{red} to the candidates for Ser14 $C_\alpha H$ in D14S-Fd_B^{ox} provide direct confirmation for this assignment. A combination of 1D and 2D NMR magnetization-transfer experiments provides the parallel assignments for D14S-Fd_A^{red} and D14S-Fd_A^{ox}, where the latter exhibits chemical shifts for each proton (except that for Cys17 $C_\beta H$) that are essentially the same as determined directly for D14S-Fd_B^{ox} (not shown; see Supporting Information). The chemical shifts and T_1 values for all assigned cluster ligand resonances from D14S-Fd^{ox} and D14S-Fd^{red} are listed in Tables 1 and 2, respectively.

Cyanide Binding to WT Fd^{red}. Addition of potassium cyanide to WT Fd_B^{red} and WT Fd_A^{red} leads to the appearance of new sets of peaks B_i^{CN} for Fd_B^{red}-CN (as shown in Figure 3D) and A_i^{CN} for Fd_A^{red}-CN (not shown; see Supporting Information) at the expense of the intensities of peaks B_i^{red} and A_i^{red}, respectively. The addition of ~100 mM KCN to a 3 mM ~1:1 mixture of Fd_A^{red} and Fd_B^{red} gives a spectrum that exhibits about 1:1 intensity ratio for $B_i^{red}:B_i^{CN}$ and $A_i^{red}:A_i^{CN}$, indicating a similar cyanide binding constant ~12 M⁻¹ for the Fd_A^{red} and
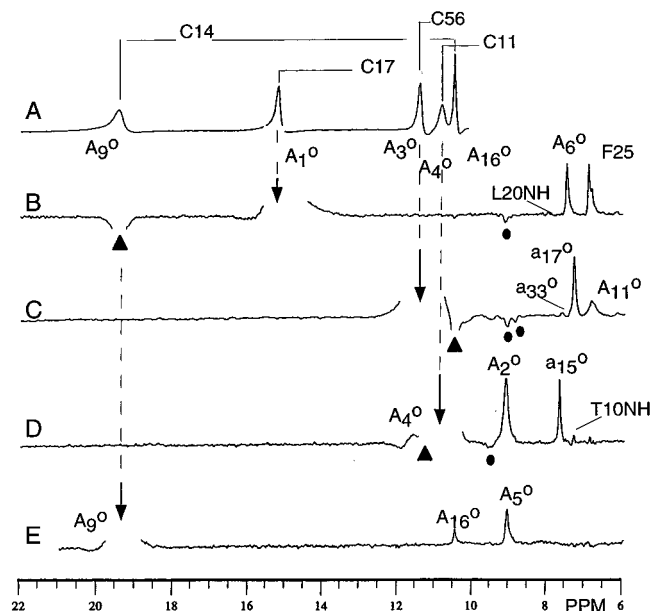
of O₂ prompted initiating the detailed assignment of D14S-Fd_B^{ox}. The assignments for the signals for the ligated Cys11, Cys17, and Cys56 by steady-state NOEs are shown in Supporting Information and leave the hyperfine-shifted signals, B_9^o and B_5^o, in Figure 7A as candidates for the unassigned Ser14. Saturation of the more strongly relaxed peak B_9^o in D14S-Fd_B^{ox} leads to a weak NOE to B_5^o, identifying $B9^o$ and $B5^o$ as the $C_\beta H_2$ of Ser14 (Figure 7B). A NOE to a nonresolved narrow peak B_{16}^o upon saturating B_5^o (Figure 7C) locates the expected contact-shifted Ser14 $C_\alpha H$.

2D EXSY data[38] on a mixture of D14S-Fd_B^{red} and D14S-Fd_B^{ox} exhibit the cross peaks that provide the assignments for

Ligation Mutants of Pyrococcus Ferredoxin

J. Am. Chem. Soc., Vol. 119, No. 40, 1997 9347

Figure 5. (A) Low-field portion of the 500 MHz ^{1}H NMR spectrum of D14C-Fd$_A^{ox}$ with peaks labeled A$_i^o$ and by sequence-specific assignment deduced herein. B−E: Steady-state NOE difference traces obtained by saturating the resonance indicated by the vertical arrow; the position of the irradiation in the reference trace is indicatd by a solid triangle and NOEs due to the reference trace are marked with solid ovals: (B) saturate A$_1^o$ (Cys17 C$_\beta$H) and observe NOE to A$_6^o$ (Cys17 C$_\alpha$H) and Phe25 ring proton; (C) saturate A$_3^o$ (Cys56 C$_\beta$H) and observe NOEs to A$_{11}^o$ (Cys56 C$_\beta$H) and a$_{17}^o$ (Cys56 N$_P$H); (D) saturate A$_4^o$ (Cys11 C$_\beta$H′) and observe NOEs to A$_2^o$ (Cys11 C$_\beta$H), a$_{15}^o$ (Cys11 N$_P$H) and Thr 10 N$_P$H; (E) saturate A$_9^o$ (Cys14 C$_\beta$H′) and observe NOEs to A$_{16}^o$ (Cys14 C$_\alpha$H) and A$_5^o$ (Cys14 C$_\beta$H).

Fd$_B^{red}$ species.[44] The T_1s for all resolved low-field resonances in WT Fd$_B^{red}$-CN (Figure 3D) and Fd$_A^{red}$-CN are considerably shorter (by a factor of ∼2−10) than found in the absence of cyanide. This extreme relaxation precluded the detection of the expected NOE between geminal partner C$_\beta$Hs (<0.5%). However, saturation of peak B$_1^{CN}$ resulted in a weak NOE to the narrowest and least relaxed resolved resonance B$_6^{CN}$, as well as to the ring of Phe25, identifying B$_1^{CN}$ and B$_6^{CN}$ as the C$_\beta$H and C$_\alpha$H of Cys17 in Fd$_B^{red}$-CN (not shown; see Supporting Information); the peak A$_1^{CN}$ and A$_6^{CN}$ were similarly assigned to Cys17. The resolved signals exhibit the relative relaxation pattern expected for Cys C$_\alpha$H and C$_\beta$Hs and give no evidence for the narrower and much less strongly relaxed signals[24] for a ligated Asp to the low field of ∼9 ppm. The signals B$_1^{CN}$, B$_6^{CN}$, B$_x^{CN}$, and B$_y^{CN}$ exhibited positive slopes (Curie-like), while B$_z^{CN}$ exhibited negative (anti-Curie) slopes in a Curie plot (not shown; see Supporting Information). The chemical shifts at 30 °C, the nonselective T_1s, and the available assignments of WT Fd$_B^{red}$-CN and Fd$_A^{red}$-CN are listed in Table 3.

Discussion

Molecular Structure of Mutant Fds. The "diamagnetic" 0−10 ppm portion of ^{1}H NMR spectra for WT and both mutant Fd$_A^{ox}$ are very similar[35] and both the chemical shifts and tertiary contacts for the assigned residues Trp2, Thr10, Val24, Phe25, Tyr46, and Ser59 are highly conserved. A similar structural conservation has been noted in a comparison of the A and B forms for WT Fd^{ox} and Fd^{red}. Cys21 and Cys48, moreover, are redox active and convert between two free sulfhydryls and a disulfide bond as described for WT *Pf* Fd,[34] with the strongly

---

(44) It is observed that small amounts of O$_2$ oxidize the sulfhydryls of Cys21 and Cys48 in preference to the cluster, indicating that the cluster potential is higher with respect to the disulfide in the cyanide derivative in Fd$_B^{red}$-CN compared to WT Fd$_B^{red}$.
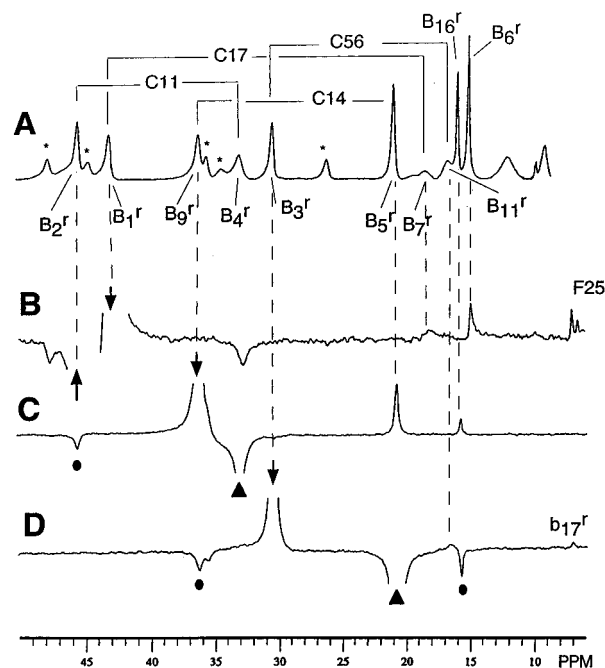

Figure 6. (A) Low-field portion of the 500 MHz ^{1}H NMR spectrum of ∼75% D14C-Fd$_B^{red}$ (peak labeled B$_i^r$): 25% D14C-Fd$_A^{red}$ (with peaks labeled by asterisks) in ^{2}H$_2$O, 50 mM in phosphate, pH 7.2 and 30 °C. The sequence-specific assignments deduced herein are also given. B−D: Steady-state NOE difference traces obtained by saturating the signal of interest as indicated by a vertical arrow: (B) saturate B$_1^r$ (Cys17 C$_\beta$H) (in positive direction) and observe NOEs (in the positive direction) to B$_7^r$ (Cys17 C$_\beta$H′), B$_6^r$ (Cys17 C$_\alpha$H), and Phe25 ring. The reference trace shows saturation of B$_2^r$ (Cys11 C$_\beta$H) and resulting NOEs to B$_4^r$ (Cys11 C$_\beta$H′); (C) saturate B$_9^r$ (Cys14 C$_\beta$H′) and yield NOEs to B$_5^r$ (Cys14 C$_\beta$H) and B$_{16}^r$ (Cys14 C$_\alpha$H); (D) saturate B$_3^r$ (Cys56 C$_\beta$H) and observe NOE to B$_{11}^r$ (Cys56 C$_\beta$H′) and b$_{17}^r$ (Cys56 N$_P$H).
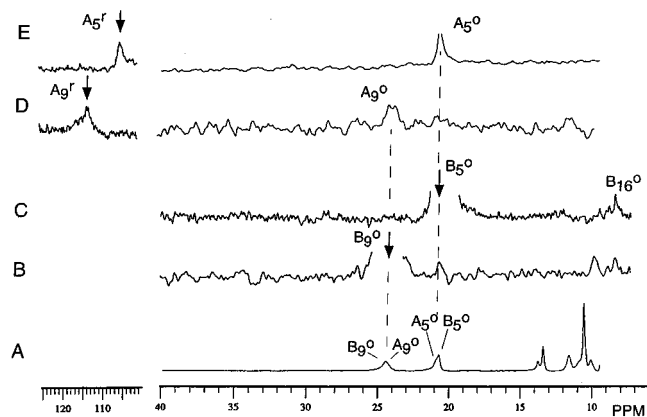

Figure 7. (A) Resolved low-field portion of the 500 MHz ^{1}H NMR spectrum of ∼75% D14S-Fd$_B^{ox}$, ∼25% D14S-Fd$_A^{ox}$, with peaks for the former complex labeled B$_i^o$, as well as by the sequence-specific assignment deduced herein (peaks A$_9^o$ and A$_5^o$ are also labeled) and (B and C) steady-state NOE difference spectra for D14S-Fd$_B^{ox}$ upon saturating the peak with the vertical arrow: (B) saturate peak B$_9^o$ (Ser14 C$_\beta$H′) in D14C-Fd$_A^{ox}$ and observe NOE to B$_5^o$ (Ser14 C$_\beta$H); (C) saturate peak B$_5^o$ (Ser14 C$_\beta$H) in D14S-Fd$_A^{ox}$ and observe NOE to peak B$_{16}^o$ (Ser14 C$_\alpha$H). (D and E) Magnetization-transfer difference spectra obtained by saturating the extreme low-field peaks A$_i^r$ of D14S-Fd$_A^{red}$ (indicated by vertical arrows) in a sample containing ∼80% D14S-Fd^{ox} and ∼20% D14S-Fd^{red} in the Fd$_A$:Fd$_B$ ratio 70:30: (D) saturate peak A$_9^r$ (and minor B$_9^r$) and observe magnetization transfer to B$_9^o$ (and minor A$_9^o$), and (E) saturate peak A$_5^r$ (Ser14 C$_\beta$H) of D14S-Fd$_A^{red}$ and observe magnetization transfer to the assigned peak A$_5^o$ (Ser14 C$_\beta$H) of D14S-Fd$_A^{ox}$.

retarded redox rate at 30 °C for the disulfide bond formation and breakage similar in the mutants and WT *Pf* Fd. Detailed descriptions of the molecular structure of these Fds should

eventually shed light on the very different electron self-exchange rates for the mutant Fd,[35] but are well outside the scope of this report.

Comparison of Mutant and WT Oxidized Cluster Fds. The location of four geminal proton pairs with significant contact shifts in each Fd^{ox} establish that residue 14 is ligated to the cluster in both mutants. The ligation of Cys11, Cys17, and Cys56 is demonstrated directly. The presence of a fourth AMX spin system with large contact shifts locates the fourth cluster ligand which sequence and structural homology to other cubane Fds demand is residue 14. Since the contact shifts for ligand 14 are pH independent in the region 6−8, we infer that only the anionic form of ligand 14 is ligated in each of the Fd. Both the magnitude and pattern of the contact shifts (Table 1), as well as the temperature dependence (not shown; see Supporting Information), of the three conserved cluster ligands Cys11, Cys17, and Cys56 are similar for the variable position-14 ligands Asp, Cys and Ser, which argues against any significant change in cluster geometry, *i.e.*, minimal changes in $f(\theta)$ in eq 1. Since Fd^{ox} has four oxidation-state equivalent irons, the relative ligand 14 contact shifts reflect the *intrinsic spin delocalization*, (*i.e.*, relative A_i in eq 1) *for each ligand due to the same* $\langle S_z \rangle$ *on the iron*. The ratios[45] of the mean $C_\beta H$ and $C_\beta H'$ contact shifts ($\sim A_i$), using the D14C-Fd^{ox} as reference (see below), for D14S-$Fd_A{}^{ox}$:D14C-$Fd_A{}^{ox}$:WT $Fd_A{}^{ox}$ are 1.5:1.0:0.2. The larger Ser14 vs Cys14 $C_\beta H$ shifts and stronger relaxation for the same $\langle S_z \rangle$ likely reflect the shorter Fe−O than Fe−S bond length and agree with similar observations for Ser mutants of both 2Fe:2S $Fd^{30,31}$ and Hipip.[32] The much smaller Asp14 than Cys14 contact shifts for the same $\langle S_z \rangle$ are due to attenuated spin transfer because of the additional intervening atom for ligated Asp,[24] as also found in models.[46]

The uniform anti-Curie behavior in the variable-temperature plots (not shown; see Supporting Information) confirm the expected $S = 0$ ground state for mutant and WT Fd^{ox} in both the A and B states, with similar, but not quite identical, population of $S = 1$ and $S = 2$ excited spin states. There are two spectral features that discriminate among the residue 14 ligands. First, the T_1s for the ligated Cys in D14C-Fd^{ox} are very similar to those for *Thermococcus litoralis, Tl,* 4Fe Fd^{ox} with Cys-only cluster ligation,[47] but generally *longer* than those for the ligated Cys in either WT[24] or D14S-Fd^{ox} (Table 1). The mean ligand $C_\beta H$ shifts for the conserved Cys11, Cys17, and Cys56 increase weakly in the order D14C-Fd $\approx$ D14S-Fd $<$ WT Fd, and the shifts, when resolved, are always larger for $Fd_A{}^{ox}$ than $Fd_B{}^{ox}$ (Table 1) indicating that the population of the $S = 1$ and $S = 2$ states is slightly greater in the same direction.

Comparison of Mutant and WT Reduced Cluster Fd. EPR spectra at 8 K of D14C-$Fd_B{}^{red}$ and D14S-$Fd_B{}^{red}$ and WT $Fd_B{}^{red}$-CN are characteristic of a $S = {}^1/_2$ ground state;[33] that for WT $Fd_B{}^{red}$ indicates $\sim25\%$ $S = {}^1/_2$ and $\sim75\%$ $S = {}^3/_2$ ground state,[22,27] although the pattern of ^1H NMR shifts at 30 °C is very similar to those exhibited by $S = {}^1/_2$ ground state [4Fe:4S]$^{1+}$ cluster.[24] The patterns of hyperfine shifts in the window 0−50 ppm are quite similar with Asp, Ser, Cys, or CN$^-$ ligated to the cluster (Figure 3), and the temperature dependence of the contact shifted $C_\beta H$s and $C_\alpha H$ are also similar with both
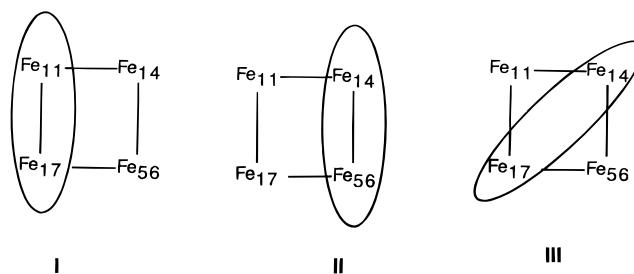

Figure 8. Schematic representation of a [4Fe:4S]$^+$ cluster with the location of the mixed valence pair $2Fe^{2.5+}$ (encircled Fes) ligated by Cys11 and Cys17 (**I**), ligand 14 and Cys56 (**II**), ligand 14 and Cys17 (**III**).

Curie and anti-Curie types present (Figure 4). The ligated Ser14, however, reveals unprecedented contact shifts in the 100−115 ppm window that are much larger than for any other ligand in a $S = {}^1/_2$ ground-state [4Fe:4S]$^{1+}$ cluster. The T_1 values for the $C_\beta H$ protons for the conserved Cys ligand protons change as a function of ligation at position 14 as follows: CN $<<$ Cys $\approx$ Ser $<$ Asp, but only the extremely short values for cyanide-ligated cluster are clearly outside the range known for any all-Cys-ligated cluster. These data suggest that the observation of anomalously short T_1s (as for cyanide) with a "normal" Cys shift pattern, or anomalously large proton contact shifts (as for ligated Ser) with "normal" relaxation can be taken as evidence for non-Cys ligand for a [4Fe:4S]$^{1+}$ cluster. However, any attempt to identify the non-Cys ligand by either T_1 and/or shift criteria would be premature. It has been shown in model compounds and proteins that numerous other ligands, including His, Tyr, H_2O, or OH$^-$, can bind to a cubane cluster,[4,19,48] and the influences of their ligation on the cluster Cys contact shifts/relaxation are not known at this time.

Electronic Structure and Magnetic Properties of D14C-$Fd_B{}^{red}$. The influences of ligand 14 on the cluster properties are analyzed first for the $Fd_B{}^{red}$ with the complete ligand $C_\beta H$ assignments. The variable-temperature behavior of the assigned Cys resonances show two (Cys11 and Cys17) with Curie-like or positive slopes and two (Cys14 and Cys56) with anti-Curie-like or negative slopes in Figure 4B. On the premise that any single cluster electronic state possesses $2Fe^{2.5+}$ and $2Fe^{2.0+}$ with associated spin states[49,50] $^9/_2$ and 4, the qualitative behavior of the resonances in Figure 4B discriminates among the four iron so that those ligated by Cys11 and Cys17 more closely resemble the $2Fe^{2.5+}$, while those ligated by Cys14 and Cys56 exhibit properties expected for ligation to $2Fe^{2.0+}$. These properties can be described in general by an equilibrium between two cluster electronic structures where the mixed-valence pair is ligated by Cys11 and Cys17 (**I** in Figure 8) or Cys14 and Cys56 (**II** in Figure 8), with the position of the equilibrium in D14C-$Fd_B{}^{red}$ in favor of **I**.

While the T_1 values for D14C-Fd^{red} are very similar to those in other isoelectronic, all-Cys ligated cluster Fd^{red}, the T_1s for individual Cys in the present mutant differ systematically. Thus it is noted in Table 2 that the T_1s for the $C_\beta H$s are longer by a

(45) The mean contact shift for $C_\beta H$ and $C_\beta H'$ were obtained by subtracting the expected diamagnetic shift (3.1 ppm for Cys, 3.9 ppm for Ser and 2.8 ppm for Asp) from the mean of the observed shifts given in Table 2, which, on the assumption of identical $\langle S_z \rangle$ and conserved $f(\theta)$ in eq 1, lead to A(Ser):A(Cys):A(Asp) = 17.8:12.2:2.3, in ppm, or the ratio 1.5:1.0:0.2.

(46) Weigel, J. A.; Holm, R. H. *J. Am. Chem. Soc.* **1991**, *113*, 4184−4191.

(47) Donaire, A.; Gorst, C. M.; Zhou, Z.-H.; Adams, M. W. W.; La Mar, G. N. *J. Am. Chem. Soc.* **1994**, *116*, 6841−6849. Donaire, A.; Zhou, Z.-H.; Adams, M. W. W.; La Mar, G. N. *J. Biomol. NMR* **1996**, *7*, 35−47.

(48) Cleland, W. E.; Holtman, D. A.; Sabat, M.; Ibers, J. A.; DeFotis, G. C.; Averill, B. A. *J. Am. Chem. Soc.* **1983**, *105*, 6021−6031. Evans, D. J.; Leigh, G. J. *J. Inorg. Biochem.* **1991**, *42*, 25−35. Evans, D. J. *Inorg. Chim. Acta* **1993**, *203*, 253−256.

(49) Both $S = {}^9/_2$, 4 and $S = {}^7/_2$, 3 spin states have been proposed[50,51] for the mixed-valence and diferrous pairs. It is noted, however, that the characteristic Curie-like and anti-Curie-like temperature dependence for $2Fe^{2.5+}$ and $2Fe^{2.0+}$, respectively, result from either the $^9/_2$, 4 or $^7/_2$, 3 spin pairs.[16]

(50) Mouesca, J.-M.; Noodleman, L.; Case, D. A.; Lamotte, B. *Inorg. Chem.* **1995**, *34*, 4347−4359. Noodleman, L.; Peng, C. Y.; Mouesca, J.-M.; Case, D. A. *Coord. Chem. Rev.* **1995**, *144*, 199−244.

(51) Telser, J.; Huang, H.; Lee, H.-I.; Adams, M. W. W.; Hoffman, B. J. *J. Am. Chem. Soc.* **1997**, submitted.

factor $\sim$2 for Cys14 and Cys56 than for Cys11 and Cys17. Similar behavior is observed[47,52] for *Tl* Fd^{red}. Thus the "Curie-like" variable-temperature behavior is linked to shorter T_1s for Cys11 and Cys17 and the "anti-Curie-like" behavior for Cys14 and Cys56 is linked to longer T_1s, precisely as expected by dipolar relaxation of protons by the $\langle S_z \rangle$ on the individual iron, with $\langle S_z \rangle$ larger for the $S = {}^9/_2$, 2Fe$^{2.5+}$ than the $S = 4$, 2Fe$^{2.0+}$ pair. This experimentally detectable difference in the strengths of the dipolar relaxation experienced by the valence-state differentiated iron pairs is important in the context of the use of paramagnetic relaxation as a constraint to generate robust molecular models for [4Fe:4S]$^+$ cluster-containing Fd with Cys-only ligation.[53,54] Similar relaxation data have not been reported for other [4Fe:4S]$^+$ Fd or any [4Fe:4S]$^{3+}$ Hipip to gauge the generality of the phenomenon.

In all cases where sequence-specific assignments for the all-Cys cluster ligands in Fd^{red} have been reported[18,47,55] the mixed-valence pair is ligated by the homologous ligands in the consensus ligation sequence (Figure 1), Cys I and Cys III. However, the available data do not yet shed light on the structural basis that makes the reduction potential of the iron pair ligated to Cys II and IV lower than the iron pair ligated to Cys I and III.

Electronic Structure and Magnetic Properties of D14S-Fd$_B$^{red}. While the mean $\langle S_z \rangle$ in eq 1 for the four irons in D14S-Fd$_B$^{red} is very similar to that in D14C-Fd$_B$^{red}, the former exhibits neither the simple pattern of ligand pairs with Curie- and anti-Curie-like temperature dependence (Figure 4B) nor the obvious asymmetry in ligand relaxation times (Table 2) observed for the reference D14C-Fd$_B$^{red}. Substitution of Ser for Cys can be viewed, in the simplest limit, as a substitution of the ligated heteroatom for a largely conserved cluster geometry, and differences in contact shifts should reflect perturbation of the relative stabilities of the 2Fe$^{2.5+}$ vs 2Fe$^{2.0+}$ iron pair ligated to Cys vs Ser. Assuming that any single electronic structure possesses a valence-delocalized iron pair and a diferrous pair, we use the *Pf* D14C-Fd$_B$^{red} mutant as the reference to which the ^{1}H NMR properties of the D14S-Fd^{red} (and later WT Fd^{red}) are compared. Conversion of an iron to a given ligand from Fe$^{2.5+}$ to Fe$^{2.0+}$ would be expected to result in a decreased positive slope (or change to negative slope) in the Curie plot and smaller contact shift, while conversion of Fe$^{2.0+}$ to Fe$^{2.5+}$ would be expected to result in less anti-Curie or negative slope (or change to positive slope) and a larger contact shift.

The major impact of replacing Cys14 in D14C-Fd$_B$^{red} with Ser14 in D14S-Fd$_B$^{red} is to make the Cys C$_\beta$H Curie-slope much less positive (and the contact shift magnitude smaller) for Cys11 and Cys17, and the slopes less negative (and contact shifts larger) for Cys56, as shown in Figure 4B and Table 2. While the Ser14 shifts cannot be directly compared to Cys14 shifts because of intrinsic difference in delocalized spin density for the same iron, the expected increase by a factor[45] of 1.5 based on the observation for D14S-Fd$_B$^{ox} and D14C Fd$_A$^{ox} predicts mean Ser14 C$_\beta$H shifts of $\sim$42 ppm in D14S-Fd$_B$^{red}, rather than the $\sim$106 ppm observed. Hence $\langle S_z \rangle$ for the Ser14 ligated iron in D14S-Fd$_B$^{ox} is significantly larger than for the Cys14-ligated

iron in D14C-Fd$_B$^{red}. It is also observed that the Curie slope for Ser14 C$_\beta$Hs in D14S-Fd$_B$^{red} is much less negative (one actually exhibits positive slope) than the Cys14 C$_\beta$Hs in D14C-Fd$_B$^{red}. This pairwise compensating change in shift magnitudes and Curie slopes is that expected for an electronic structure intermediate between that described by **I** and **II** in Figure 8 (*i.e.*, **I** and **II** are comparably populated). Thus the ligated Ser favors the higher iron oxidation state when compared to Cys.

Analysis of the nature of the magnitude and slope in a Curie plot of the Ser vs Cys contact shifts in WT *Chromatium vinosum* Hipip^{ox} and its C77S-Hipip^{ox} ([4Fe:4S]$^{3+}$) mutant, has shown that the substitution of Ser for Cys ligated to a valence-delocalized Fe$^{2.5+}$ converts the iron ligated to ligand 77 to one of the 2Fe$^{3.0+}$ pair.[32] In that context, the Ser for Cys mutation in both the Fd and Hipip cubane clusters supports the assertion that Ser ligation favors the higher oxidation state of iron, one of 2Fe$^{2.5+}$ in Fd^{red} and one of 2Fe$^{3.0+}$ in Hipip^{ox}. A difference between the response of Hipip^{ox} and *Pf* Fd^{red} to a Cys to Ser substitution is that, in the former, primarily the site of the iron to ligand 77 is influenced,[32] while in the latter, the substitution alters similarly the state of *a pair of irons*. In contrast, replacement of a Cys ligated to Fe$^{2.0+}$ in *Anabaena* 2Fe Fd failed to convert[30,31] it to the Fe$^{3.0+}$. Mutagenesis experiments are in progress, and NMR studies are planned on a series of *Pf* Fd^{red} double mutants D14C, together with C11S, C17S, or C56S. These studies should shed further light on whether the effect of the variable position Cys to Ser substitution can be interpreted on the basis of the same model described above or whether the effect of Cys to Ser substitution depends on the position of the Cys in the conserved ligating sequence.

Electronic Structural and Magnetic Properties of WT Fd$_B$^{red}. The patterns of contact shifts (Table 2) and Curie slopes (Supporting Information) for the four ligands in WT Fd$_B$^{red} are more complicated than that for either D14C-Fd$_B$^{red} or D14S-Fd$_B$^{red}. Scaling the ligated Asp14 contact shift by the intrinsic ratio[45] determined for Fd^{ox} shows that $\langle S_z \rangle$ on the Asp14 ligated Fe in WT Fd$_B$^{red} is much larger (by a factor of $\sim$2$-$3) than for the Cys14 ligated Fe in D14C-Fd, and hence the mean cluster $\langle S_z \rangle$ for the four iron *appears to be larger* than for either D14C-Fd$_B$^{red} or D14S-Fd$_B$^{red}. Whether this larger mean $\langle S_z \rangle$ is due to weaker antiferromagnetic coupling, and hence more extensive population of excited $S = {}^3/_2$, $^5/_2$, etc. states, or whether there are both $S = {}^1/_2$ and $S = {}^3/_2$ ground states, as observed at 4 K by EPR,[22,9,27,51] is not known at this time. However, comparison of changes in Curie slope and shift magnitude for WT Fd$_B$^{red} with D14C Fd$_B$^{red} allows several conclusions.

The change in slope from anti-Curie for Cys14 in D14C-Fd$_B$^{red} (Figure 4A) to Curie for Asp14 in WT Fd$_B$^{red}, together with the increased $\langle S_z \rangle$ for the iron ligated by residue 14 (Table 2), dictates that *Asp14 is ligated to a valence-delocalized iron* in WT Fd$_B$^{red}. Similarly, the characteristic decrease in C$_\beta$H contact shifts for Cys11, and the change from Curie to anti-Curie, upon replacing Cys14 by Asp14 clearly dictates that Cys11 is ligated to a Fe$^{2.0+}$ in WT Fd$_B$^{red}. The consequences of Asp for Cys substitution for the remaining two ligands can be qualitatively interpreted by considering primarily the changes in Curie slope for the relevant residues. The Cys17 shift magnitudes are perturbed little, but the Curie slope becomes less positive (in fact, almost zero slope; see Supporting Information) upon replacing Cys14 by Asp14, indicating that the *oxidation state of the Cys17-ligated iron is lowered* in WT relative to that in D14C Fd^{red}, but not completely to that of Fe$^{2.0+}$. The Cys56 contact shifts are also perturbed minimally, but the slopes are less negative in WT relative to those of D14C Fd$_B$^{red}, indicating that the ligated *iron oxidation state has increased*, but not up to Fe$^{2.5+}$. The Curie slopes of Cys17

(52) The T_1 values (in ms) for the C$_\beta$Hs of the ligated Cys in *Thermococcus litoralis*[47] Fd^{red} have been redetermined from the intial rates of magnetization recovery in an inversion$-$recovery experiment ($\pm$15% uncertainty), CysI (7,3), CysII(15,6), CysIII(11,3) and CysIV(13,5) for the C$_\beta$H and C$_\beta$H$'$ protons.

(53) Huber, J. G.; Moulis, J.-M.; Gaillard, J. *Biochemistry* **1996**, *35*, 12705$-$12711.; Bertini, I.; Couture, M. M. J.; Donaire, A.; Eltis, L. D.; Felli, I. C.; Luchinat, C.; Piccioli, M.; Rosato, A. *Eur. J. Biochem.* **1996**, *241*, 440$-$452.

(54) Wang, P. L.; Donaire, A.; Zhou, Z.-H.; Adams, M. W. W.; La Mar, G. N. *Biochemistry* **1996**, *35*, 11319$-$11328.

(55) Lebrun, E.; Simenel, C.; Guerlesquin, F.; Delepierre, M. *Magn. Res. Chem.* **1996**, *34*, 873$-$880.

and Cys56 signals in WT Fd_B^{red}, in fact, are intermediate between those for a mixed-valence and ferrous iron.

On the assumption that any single electronic structure has $2Fe^{2.5+}$ and $2Fe^{2.0+}$, the WT Fd_B^{red} electronic structure is consistent with the presence of the two comparably populated structures **II** and **III** depicted in Figure 8. The schematic electronic structures **II** and **III** for WT Fd_B^{red} in Figure 8 indicate that ligation by Asp stabilizes the valence-delocalized pair at that position relative to Cys, but more strongly than Ser, since both **II** and **III** ligate Asp14 to a $Fe^{2.5+}$, while only one (**II**) of two structures comparably populated ligated Ser14 to a $Fe^{2.5+}$. The ligation of Asp14 to an iron of the mixed-valence $Fe^{2.5+}$ rather than $Fe^{2.0+}$ is consistent with the proposal based on analysis of the low-temperature EPR and ENDOR spectra[27,51] of WT Fd^{red} selectively reconstituted with ^{57}Fe. The low-temperature ENDOR data[51] favor the $^7/_2$, 3 rather than $^9/_2$, 4 sub-spin states for $2Fe^{2.5+}$ and $2Fe^{2.0+}$, respectively, for the total spin $^1/_2$ ground state[49] and do not differentiate between structures II and III in Figure 8. Whether the increased mean iron $\langle S_z \rangle$ detected by NMR for WT *Pf* Fd^{red} arises from weaker antiferromagnetic coupling for a $S = ^1/_2$ ground state formed from $S = ^7/_3$, 3 sub-spin systems[51] or if it is due to the presence of both $S = ^1/_2$ and $S = ^3/_2$ ground states[27] cannot be determined from the presently available data.

Influence of Cys21 and Cys48 Oxidation States on Reduced Cluster Electronic Structure. Comparison of the shifts in Table 2 and the Curie plots for $D14C$-Fd_A^{red} (Figure 4A) and $D14C$-Fd_B^{red} (Figure 4B) show Curie- and anti-Curie slopes for the same Cys11, Cys17 and Cys14, Cys56, respectively. However, the Curie slopes are more positive and the shifts larger, while the anti-Curie peak shifts are smaller, in $D14C$-Fd_A^{red} than $D14C$-Fd_B^{red}. Very similar changes in Curie slope and shift magnitude (Table 2) are observed for the pairwise Cys11, Cys17 and Cys56, Ser14 in $D14S$-Fd_B^{red} (Figure 4B) relative to $D14S$-Fd_A^{red} (Figure 4A). These data indicate that an equilibrium between the same two structures, **I** and **II** in Figure 8, describes the mutant Fd_A^{red} electronic structures, except that in each case the *free sulfhydryl Fd_B^{red} form of Cys21 and Cys48 favors structures **II** over **I** (Figure 8) for both mutants when compared to the disulfide form (Fd_A^{red}) of Cys21 and Cys48.* For WT Fd^{red}, one mixed-valence $Fe^{2.5+}$ (to Asp14) is conserved (unchanged shift (Table 2) and Curie slope), while each of the other ligands shows moderate changes in shifts that indicate that the oxidation state of the iron ligated to Cys17 increases (more positive Curie slope) while that ligated by Cys56 decreases (less positive slope) for the disulfide relative to the free sulfhydryl form of Cys21 and Cys48.

Clearly the redox states of Cys21 and Cys48 are sensed by the cluster such that the iron pair ligated to Cys17 and Cys11 is more reducible for the free sulfhydryl than disulfide form of Cys21 and Cys48. In the crystal structures of *Desulfovibrio gigas*[56] 3Fe Fd^{ox} and *Thermatoga maritima*[57] 4Fe Fd^{ox}, as well as in the solution structure of *Thermococcus litoralis*[54] 4Fe Fd^{ox}, each of which has a disulfide bond between CysV and CysVI, the carbonyl of cluster ligand **III** (Cys17 in *Pf* Fd) serves as a hydrogen-bond acceptor to the peptide NH of CysV (Cys21 in

Pf Fd). We propose that an analogous hydrogen bond exists in *Pf* Fd. Solution structure determinations of both *Pf* Fd_A and Fd_B that may shed light on the nature of the interaction between the two redox chromophores, are in progress. It is noted that the cluster reduction potential is not significantly perturbed[34] by the oxidation states of Cys21 and Cys48.

Effect of Cyanide Ligation to the Cluster. Perhaps the most unusual property of the Fd^{red}-CN complex is the extremely effective relaxation of conserved cluster ligand[58] Cys relative to that in the two mutants and WT Fd^{red}. A longer electron spin relaxation time, T_{1e}, for *Pf* Fd^{red}-CN compared to WT Fd^{red} is implied by the ability to detect the $S = ^1/_2$ EPR signal at higher temperature in the presence, than in the absence, of cyanide.[27] The short proton T_1s from the hyperfine-shifted signals in Fd^{red}-CN preclude detection of NOEs between geminal C_βHs, but the NOEs from the strongly relaxed B_1^{CN} (or A_1^{CN}) to the narrow B_6^{CN} (or A_6^{CN}) and to Phe25 clearly assign the Cys17 C_βH and C_αH. The three other hyperfine-shifted peaks, B_x^{CN}, B_y^{CN}, and B_z^{CN}, cannot be unambiguously assigned at this time, but it is noted that WT Fd^{red} similarly has only three hyperfine-shifted resonances beside the Cys17 C_βH downfield of ~20 ppm,[24] two from Cys11 and one from Cys56, and a similar origin for the peaks in Fd^{red}-CN is likely. Moreover, since two peaks (B_x^{CN} and B_y^{CN}) exhibit Curie, while one peak (B_z^{CN}) displays anti-Curie behavior (not shown, see Supporting Information), a tentative assignment is B_x^{CN} and B_y^{CN} to the C_βHs of Cys11 and B_z^{CN} to the C_βH of Cys56. Since Cys17 and the likely Cys11 exhibit Curie-type behavior, and Cys56 exhibits anti-Curie behavior, an electronic structure is proposed where Cys11 and Cys17 are ligated to the mixed valence pair, and Cys56 and cyanide to the $2Fe^{2.0+}$ pair, *i.e.*, an electronic structure similar to that proposed for $D14C$-Fd_A^{red} (**I** in Figure 8). The failure to detect any hyperfine-shifted peaks with relaxation properties expected for a ligated Asp14 are consistent with, but not proof for, cyanide replacing Asp14. The conversion of a mixed valence to a ferrous iron upon cyanide ligation is completely consistent with the interpretation of EPR and ENDOR data.[27,51]

Supporting Information Available: Ten figures (Curie plots for Fd^{ox} and Fd^{red}-CN, effect of CN^- on WT Fd^{red} spectra; labels of mutant Fd_A^{red}, MCOSY map of $D14C$-Fd_A^{ox}; saturation transfer for $D14C$ Fd^{ox}/Fd^{red}, NOEs for $D14S$-Fd_B^{ox}; EXSY map for $D14S$-Fd_B^{ox}/Fd^{red}; NOEs in WT Fd_B^{red}-CN) and one table (shifts for select noncluster ligated residues) (11 pages). See any current masthead page for ordering and Internet access instructions.

JA9715455

(56) Kissinger, C. R.; Sieker, L. C.; Adman, E. T.; Jensen, L. H. *J. Mol. Biol.* **1991**, *219*, 693−715.

(57) Macedo-Ribeiro, S.; Darimont, B.; Sterner, R.; Huber, R. *Structure* **1996**, *4*, 1291−1300.

(58) The significantly enhanced relaxation of the ligated Cys C_βHs in *Pf* Fd^{red}-CN relative to WT and mutant *Pf* Fd^{red} may result, in part, from relaxation by delocalized spin density at a sulfur, since nonligated residue protons (*i.e.*, Val24 $C_\gamma H_3$) exhibit very similar T_1s ~400 ms in Fd^{red}-CN and WT Fd^{red}.